

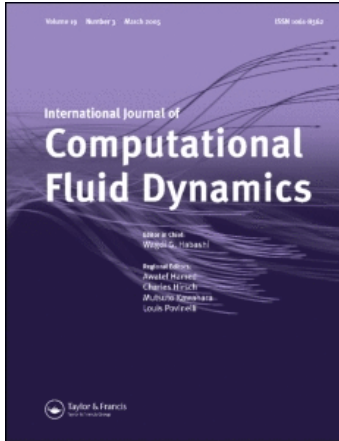
This article was downloaded by: [UJF - INP Grenoble SICD 1]

On: 2 September 2010

Access details: Access Details: [subscription number 910277717]

Publisher Taylor & Francis

Informa Ltd Registered in England and Wales Registered Number: 1072954 Registered office: Mortimer House, 37-41 Mortimer Street, London W1T 3JH, UK



## International Journal of Computational Fluid Dynamics

Publication details, including instructions for authors and subscription information:

<http://www.informaworld.com/smpp/title~content=t713455064>

### Transport properties of heterogeneous materials. Combining computerised X-ray micro-tomography and direct numerical simulations

Viivi Koivu<sup>a</sup>; Maxime Decain<sup>bc</sup>; Christian Geindreau<sup>b</sup>; Keijo Mattila<sup>a</sup>; Jean-Francis Bloch<sup>b</sup>; Markku Kataja<sup>a</sup>

<sup>a</sup> Department of Physics, University of Jyväskylä, Jyväskylä, Finland <sup>b</sup> Papermaking Process Laboratory of Grenoble, St Martin D'Herès, Grenoble, France <sup>c</sup> Laboratory 3S-R, University of Grenoble-CNRS, Grenoble, France

Online publication date: 16 April 2010

**To cite this Article** Koivu, Viivi , Decain, Maxime , Geindreau, Christian , Mattila, Keijo , Bloch, Jean-Francis and Kataja, Markku(2009) 'Transport properties of heterogeneous materials. Combining computerised X-ray micro-tomography and direct numerical simulations', International Journal of Computational Fluid Dynamics, 23: 10, 713 – 721

**To link to this Article:** DOI: 10.1080/10618561003727512

**URL:** <http://dx.doi.org/10.1080/10618561003727512>

## PLEASE SCROLL DOWN FOR ARTICLE

Full terms and conditions of use: <http://www.informaworld.com/terms-and-conditions-of-access.pdf>

This article may be used for research, teaching and private study purposes. Any substantial or systematic reproduction, re-distribution, re-selling, loan or sub-licensing, systematic supply or distribution in any form to anyone is expressly forbidden.

The publisher does not give any warranty express or implied or make any representation that the contents will be complete or accurate or up to date. The accuracy of any instructions, formulae and drug doses should be independently verified with primary sources. The publisher shall not be liable for any loss, actions, claims, proceedings, demand or costs or damages whatsoever or howsoever caused arising directly or indirectly in connection with or arising out of the use of this material.

## Transport properties of heterogeneous materials. Combining computerised X-ray micro-tomography and direct numerical simulations

Viivi Koivu<sup>a\*</sup>, Maxime Decain<sup>b,c</sup>, Christian Geindreau<sup>b</sup>, Keijo Mattila<sup>a</sup>, Jean-François Bloch<sup>b</sup> and Markku Kataja<sup>a</sup>

<sup>a</sup>Department of Physics, University of Jyväskylä, Jyväskylä, Finland; <sup>b</sup>Papermaking Process Laboratory of Grenoble, St Martin D'Herès, Grenoble, France; <sup>c</sup>Laboratory 3S-R, University of Grenoble-CNRS, Grenoble, France

(Received 24 February 2009; final version received 22 February 2010)

Feasibility of a method for finding flow permeability of porous materials, based on combining computerised X-ray micro-tomography and numerical simulations, is assessed. The permeability is found by solving fluid flow through the complex 3D pore structures obtained by tomography for actual material samples. We estimate overall accuracy of the method and compare numerical and experimental results. Factors contributing to uncertainty of the method include numerical error arising from the finite resolution of tomographic images and the rather small sample size available with the present tomographic techniques. The total uncertainty of computed values of permeability is, however, not essentially larger than that of experimental results. We conclude that the method provides a feasible alternative for finding fluid flow properties of the kind of materials studied. It can be used to estimate all components of permeability tensor and is useful in cases where direct measurements are not achievable. Analogous methods can be applied to other modes of transport, such as diffusion and heat conduction.

**Keywords:** permeability; X-ray micro-tomography; porous media; numerical methods; lattice-Boltzmann; finite difference

### Introduction

An important problem in analysing and modelling many complex natural and industrial processes is to determine realistic effective material laws and values of material parameters that would properly represent, e.g. the relevant transport properties of materials involved. Various methods ranging from purely experimental correlations to modelling based on fundamental microscopic dynamics, and lately also to numerical simulation, have been used (see e.g. Saar and Manga (1999), Belov *et al.* (2003), Lundström *et al.* (2004), Arns *et al.* (2004), Kerwald (2004), Levitz (2005), Nordlund *et al.* (2005), Verleye *et al.* (2005), Eker and Akin (2006), Keehm *et al.* (2006), Hellström and Lundström (2006), Lundström *et al.* (2006), White *et al.* (2006), Verleye *et al.* (2007), Jaganathan *et al.* (2007), Nordlund and Lundström (2007), Vidal *et al.* (2008), Andersson *et al.* (2009) and Frishfelds *et al.* (2009)). An essential factor affecting properties of many heterogeneous and porous materials is their specific internal microscopic or mesoscopic structure. That structure is often very complex and difficult to characterise in a manner that would readily be used in correlating structural and transport properties of these materials.

Computerised X-ray micro-tomography (CX $\mu$ T) techniques based on synchrotron radiation sources have been used in probing the internal structure of heterogeneous materials for more than a decade. The techniques involve taking a large number of X-ray images of the material sample from different angles. Within the so called absorption mode imaging, numerical reconstruction algorithm is then used to obtain the 3D spatial distribution of X-ray absorption coefficient which closely correlates with the local density distribution. Visualisation of this distribution gives the 3D 'image' of the material. During the recent years, the method has become more feasible as also table-top tomographic scanners utilising X-ray tubes and capable of resolution in the sub-micron range have become available. Indeed, the utilisation of non-destructive 3D examination using CX $\mu$ T techniques has opened new perspectives in heterogeneous materials research (see e.g. Thibault and Bloch (2002), Manwart *et al.* (2002), Aaltosalmi *et al.* (2004), Ramaswamy *et al.* (2004), Rolland du Roscoat *et al.* (2005), Hyvälouma *et al.* (2006) and Fourie *et al.* (2007)). Analysis of structural properties such as total amount and spatial distribution of various material components, porosity and pore size distribution, specific surface area, etc. are typical and rather straightforward examples of application of

\*Corresponding author. Email: viivi.koivu@phys.jyu.fi

CX $\mu$ T. Combining X-ray tomography with numerical simulation enables more advanced analysis of also dynamic characteristics such as transport and elastic properties of materials. An important advantage of the method is that various analyses of quite different nature can be made based on the same basic data – the 3D digital image of the material structure. The objective of this work is to develop and evaluate a method for characterising the properties of fluid flow through porous materials by combining tomographic techniques with numerical simulations in the micro-scale. More precisely, the method is applied in finding flow permeability of selected fibrous porous materials.

The flow permeability coefficient  $\mathbf{k}$  is generally a tensor valued measure of the ability of a porous material to transmit fluids. It is defined for slow, steady-state, isothermal, Newtonian fluid flow through a porous medium by Darcys's law (Darcy (1856); see e.g. Bear (1972))

$$\vec{q} = -\frac{1}{\mu} \mathbf{k} \cdot \nabla \varphi, \quad (1)$$

where  $\vec{q}$  is the (superficial) volume flux vector,  $\mu$  is the dynamic viscosity of the fluid,  $\nabla \varphi = \nabla p - \rho \vec{g}$ ,  $p$  is the pressure,  $\rho$  is the density of the fluid and  $\vec{g}$  is the acceleration due to a body force. In what follows, we concentrate on diagonal components of  $\mathbf{k}$  and apply Equation (1) in cases where  $-\nabla \varphi$  is in the direction of mean flow that takes place in three mutually perpendicular coordinate directions (to be defined later). In this case, Equation (1) is reduced in a diagonal component form as

$$q_j = -\frac{k_{jj}}{\mu} \frac{\partial \varphi}{\partial x_j}, \quad j = 1, 2, 3. \quad (2)$$

In principle, permeability coefficients for a given material sample can be found by numerically solving incompressible creeping Newtonian flow through the 3D pore space obtained by CX $\mu$ T. Obviously, the key issue in such an approach is the accuracy by which the actual pore structure of the medium can be reproduced by tomographic techniques. This accuracy is affected by properties of the CX $\mu$ T hardware used; its spatial resolution in particular, choice of imaging parameters and by 3D image post-processing methods that may be used to enhance image quality. Many natural and man-made porous materials are heterogeneous showing variation of properties in multiple scales. Large enough samples should thus be used in order to obtain statistically meaningful results. In practice, this may necessitate compromising between high resolution and large sample size.

The finite resolution of the tomographic image, as set by hardware limitations or by trade-off between

resolution and sample size, also sets a practical upper limit for the useful density of the grid for numerical solution of flow. In this work, we use most straightforward method for grid generation in which the numerical grid is a regular cubic lattice based on the tomographic image itself. The unit cell of the grid thus equals the cubic 'voxel' of the digital tomographic image. In order to estimate the accuracy of the solution obtained using such a relatively coarse numerical grid, we first compute the values of permeability coefficients for a model porous material that consists of regular lattice of straight cylinders for which also analytical results can be found. In the next step, we apply the methods in two heterogeneous fibrous materials, namely plastic felt and hardwood paper. A table-top CX $\mu$ T device and a tomographic imaging facility based on synchrotron radiation were used to obtain tomographic images for felt and paper samples, respectively. The numerical values of flow permeability obtained using the numerical grids based on these tomographic images were compared with experimental results of permeability for the same materials.

In this work, creeping flow through the pore space of materials was solved using the lattice-Boltzmann method (LBM). It is based on solving the discrete Boltzmann equation instead of the standard continuum flow equations. The solution thus yields velocity distribution function which is then used to obtain hydrodynamic variables as its moments (Succi 2001). The standard LBM involves an explicit time iteration scheme with a constant time step, uniform grid and local data dependencies. It is ideal for parallel computing. As demonstrated earlier (Succi *et al.* 1989, Koponen *et al.* 1998, Manwart *et al.* 2002, Martys and Hagedorn 2002, Belov *et al.* 2003, Kerwald 2004, Eker and Akin 2006, Kutay *et al.* 2006, Pan *et al.* 2006, White *et al.* 2006, Vidal *et al.* 2008), the LBM is particularly well suited for solving fluid flow in complex geometries such as in the pore space of irregular porous media. This advantage of the method follows mainly from straightforward implementation of the no-slip boundary condition on fluid–solid interface. Here, we use the standard halfway bounce-back boundary condition. Furthermore, we use the particular D3Q19 implementation of LBM with the linear two relaxation time approximation of the Boltzmann equation introduced by Ginzburg *et al.* (2008). It appears that this approach avoids the problem of dependence of permeability on viscosity that is encountered within more simple models such as the single relaxation time Bhatnagar-Gross-Krook (BKG) model (Ginzburg and d'Humieres 2003, Ginzburg 2008). Within LBM, a simple regular grid that consists of the centre points of the cubic unit cells (voxels of the tomographic image) was used.

The finite difference method (FDM) implemented in the Geodict software (<http://www.geodict.com>) was used for reference in solving the flow through the regular geometries and for selected porous material samples. Within this method a staggered grid was used where the values of velocity and pressure were given at centre points of the faces and volume of the cubic unit cells, respectively. The partial differential equations for incompressible Stokes flow are solved by using the 'FFF-Stokes solver' based on Fast Fourier Transform. This solver appears to be fast and memory efficient for large computations characteristic to the present approach (Wiegmann 2007).

### Estimate of discretisation error for regular geometries

As stated above, a major potential source of uncertainty within the present approach is the numerical error caused by the finite resolution of the tomographic images and thus, of the numerical grids used. Here, we wish to estimate the order of magnitude of this error by solving the flow through regular model porous materials with varying values of porosity. Solutions are found for numerical grids of different sizes and the resulting values of permeability coefficient are compared also with analytical results. To this end, we find numerical solution of flow through regular geometries that consist of square array of parallel straight rods aligned in the  $z$  direction at four different porosity levels (0.6, 0.7, 0.8 and 0.9). For each such geometry, incompressible creeping flow is induced by a small but otherwise arbitrary constant body force  $\rho\vec{g}$  in  $x$  and  $z$  coordinate directions (see Figure 1). Periodic boundary conditions were used at the boundary of the computation region in all coordinate directions and no-slip boundary condition was enforced at all solid–fluid interfaces. Numerical values of the diagonal elements of the permeability tensor were then calculated from Equation (2) using the mean flow rate given by the numerical solution. Notice that due to symmetry

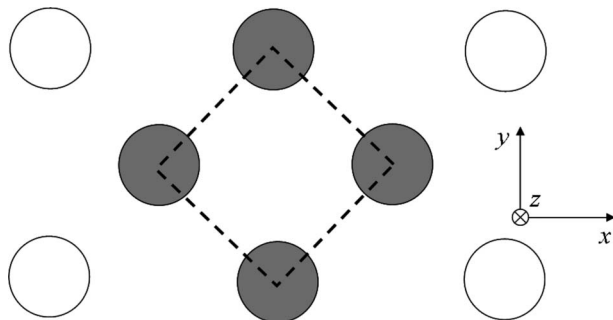


Figure 1. Unit cell of a square array of parallel rods with circular cross-section together with the coordinate convention used.

reasons the permeability tensor is isotropic in the  $x$ - $y$  plane, and that  $z$  direction is one of its principal directions. The diagonal elements  $k_{xx}$ ,  $k_{yy}$  ( $=k_{xx}$ ) and  $k_{zz}$  are thus also the principal values of the permeability tensor.

The solution was found using a high-density grid and a low-density grid. For the high-density grid the length of the unit cell was 400 grid units. This was high enough resolution to provide an accurate solution and an adequate independence of the actual grid size. For the low-density grid the diameter of the rods was 7 grid units, which equals the mean diameter of the actual fibres of the plastic felt sample measured in units of image voxel size (see below). Example of solved flow field using high and low density grids is shown in Figure 2 for mean flow in the  $x$  direction.

A number of analytical results have been derived for permeability of arrays of cylinders with circular cross section and for flow parallel and perpendicular to the cylinders (see e.g. Jackson and James (1986) and references therein). For flow parallel to the cylinders ( $z$ -direction), Drummond and Tahir (1984) propose an approximative formula

$$\frac{k_{zz}}{r^2} \approx \frac{1}{4(1-\phi)} \left( -\ln(1-\phi) - K + 2(1-\phi) - \frac{1}{2}(1-\phi)^2 \right), \quad (4)$$

where  $\phi$  is porosity,  $r$  is radius of the cylinders and  $K$  is a constant that depends on array geometry. For a square array it has the value 1.476. Equation (4) is useful at least in the porosity range  $0.3 < \phi < 0.99$ . Sangani and Acrivos (1982) used a unit cell approach to find an exact solution for flow perpendicular to the cylinders ( $x$ - $y$  plane). Their solution was given in terms of series expansions where the effect of boundary conditions must be found numerically. This result can not be expressed in closed form, but Sangani and Acrivos provide tabulated numerical results that can be readily applied in the present case.

The computed results for permeability obtained with high and low density grids for square array of circular cylinders at different values of porosity are shown in Figure 3 together with corresponding theoretical results. The numerical results obtained using the high density grid closely agree with the theoretical predictions. The numerical results obtained with the low-density grid deviate from the theoretical and more accurate numerical results. Including all the cases analysed, the maximum relative deviation between the values of permeability obtained using low-density numerical grid as compared to either theoretical or high resolution numerical results was less than 10%. In addition to results shown in Figure 3, similar

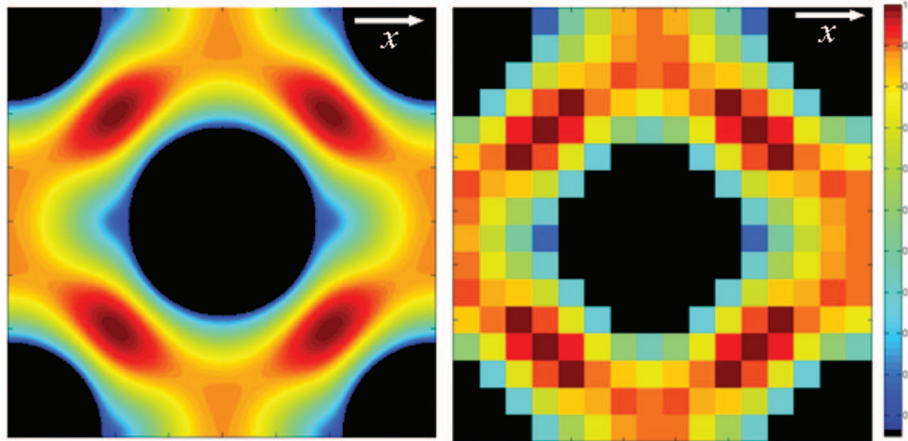


Figure 2. Flow speed solved using high density grid (a) and low density grid (b) for an array of circular cylinders (porosities 70% and 71%, respectively). The mean flow is in the  $x$  direction. Red and blue colours indicate high and low flow speed, respectively. Available in colour online.

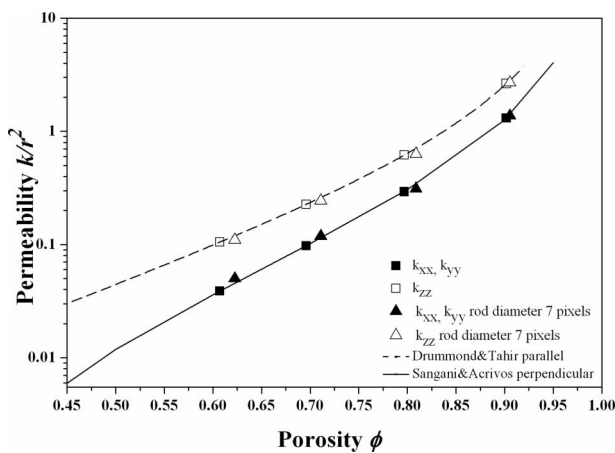


Figure 3. Numerical and analytical values of dimensionless permeability in three principal directions for square array of circular cylinders at different porosity levels. Analytical values for flow parallel to the cylinders ( $z$  direction) are given by Equation (4) and the semi-analytical results for flow perpendicular to the cylinders (in  $x$ - $y$  plane) by tabulated results of Sangani and Acrivos, see Tables 1 and 2 in Sangani and Acrivos (1982).

results were obtained for hexagonal arrays of circular rods. This analysis was also repeated for square and hexagonal arrays of rods with square cross-section. In this case, theoretical results are not available but accurate numerical solution can be found using sufficiently dense grid. Finally, the numerical results obtained with LBM were verified independently using FDM for a subset of regular geometry cases.

### Permeability of porous materials

We apply the analysis discussed in the previous sections for samples of fibrous porous materials, i.e.

felt made of plastic fibres and hand sheet paper made of chemical hardwood pulp. The actual microscopic pore geometry of the samples was obtained by CX $\mu$ T. The results will be compared with experimental data for the same materials. The felt material consists of nearly cylindrical smooth fibres of average diameter 34  $\mu$ m. The fibres are curved to some extent and have only weak tendency to be oriented in the plane of the felt. Within that plane, the orientation is isotropic, in average. The structure of paper and the internal shape of individual wood fibres are considerably more complicated than those of plastic felt. Wood fibres typically include a lumen and a cell wall with flattened irregular cross-section. The wall thickness and the average diameter of the fibres were found to be approximately 4  $\mu$ m and 20  $\mu$ m, respectively. The fibres are strongly oriented towards the plane of paper but are also isotropically oriented within that plane (Rolland du Roscoat *et al.* 2007).

The tomographic image of a plastic felt sample used in this work was obtained using a table-top tomographic scanner (SkyScan 1172) with voxel resolution 4.84  $\mu$ m. The scanned felt sample was a circular section of diameter 6 mm. In order to reproduce the internal structure of paper material in comparable detail, considerably higher resolution must be used. The paper sample used in this work was scanned at ID19 laboratory at European Synchrotron Radiation Facility (ESRF, Grenoble, France) with a voxel size of 0.7  $\mu$ m. In this case, the sample was a rectangular section of size 1.4  $\times$  1.4 mm<sup>2</sup>. The samples were carefully cut from larger sheets of felt and paper to avoid any damage to the structure due to cutting. The locations from which the samples were extracted were selected using a grey-scale transillumination image, such that the samples would represent

the mean properties (especially density) of the material as closely as possible. Both samples were scanned slightly compressed in the  $z$  direction. Compression was obtained by plastic tubular sample holders including a piston and a screw. The size of the original tomographic grey scale images was  $1240 \times 1240 \times 277$  voxels and  $2000 \times 2000 \times 121$  voxels for the felt and paper samples, respectively. The image of the felt sample was processed with variance-weighted mean filter (Gonzales and Woods 2001) before thresholding to a binary image. For this sample, thresholding was rather straightforward due to high quality of the tomographic image and regular shape of the plastic fibres. The image of the paper sample was denoised by nonlinear anisotropic diffusion filter and further thresholded using seeded region growing method (Rolland du Roscoat *et al.* 2005). The thickness and porosity of the samples were determined from the filtered and segmented tomographic images (and the same values of thickness were used in experimental measurement of permeability, see below). Porosity was determined as the total proportion of open void space in the tomographic subsamples. The values of porosity thus found were 61.6% for the felt and 48.6% for the paper sample.

For numerical flow solution, five non-overlapping subvolumes were extracted from the original tomographic images. The dimensions of these subvolumes were  $400 \times 400 \times 277$  pixels (physical size  $1930 \times 1930 \times 1341 \mu\text{m}^3$ ) and  $300 \times 300 \times 121$  pixels (physical size  $210 \times 210 \times 85 \mu\text{m}^3$ ) for the felt and paper samples, respectively. Visualisation of one of the subvolumes used in numerical analysis for felt and paper are shown in Figure 4. Numerical solution of flow through all the subsamples with mean flow in the three coordinate directions was then obtained. With the sizes of subsamples given above, the total central processing unit (CPU) time required for solution varied between 2 and 6 h in HP Proliant

DL145G2 1.8 GHz with 8 GB random access memory (RAM) nodes. Figure 5 illustrates the flow velocity fields on a single 2D layer inside the subsamples shown in Figure 4. The detailed 3D numerical solution was then used to find the values of the diagonal components of permeability tensor for the subsamples as in the case of regular geometries.

Experimental values of permeability were obtained by using a permeability measurement device (PMD) constructed originally for measuring transverse permeability ( $k_{zz}$ ) of soft porous sheet-like samples under mechanical compression (Koivu *et al.* 2009a). For the present purpose, the device was modified such that also in-plane measurement ( $k_{xx}$ ,  $k_{yy}$ ) is possible (Koivu *et al.* 2009b). Both liquids and gases can be used as permeating fluids. In transverse flow measurement, a circular sample sheet of diameter 90 mm is placed between smooth sintered stainless steel compression plates having a central area of diameter 60 mm open for flow. For in-plane measurements, a rectangular sample sheet of size 70 mm  $\times$  5 mm was sealed between solid stainless steel compression plates that allow lateral flow through the sample. The samples were then compressed to the same thickness (porosity) as the samples scanned by X-ray tomography. Experiments were conducted with air flow in order to prevent structure changes due to swelling. All measurements were repeated for five macroscopically identical samples.

Numerical and experimental results of permeability in three orthogonal directions for plastic felt and hardwood paper samples are summarised in Table 1. Notice that in this case, the values given in Table 1 are not necessarily the principal values of permeability tensor but merely the values of diagonal elements in the selected coordinate system. In this case the numerical results obtained by the two methods, LBM and FDM, deviate from each other more than in the case of regular arrays. Most likely, this is just an

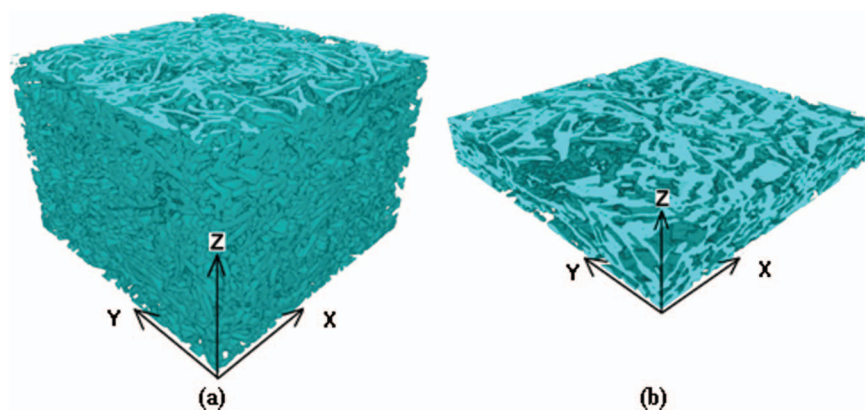


Figure 4. 3D rendering of tomographic images of plastic felt (a) and hardwood paper (b) subsamples.

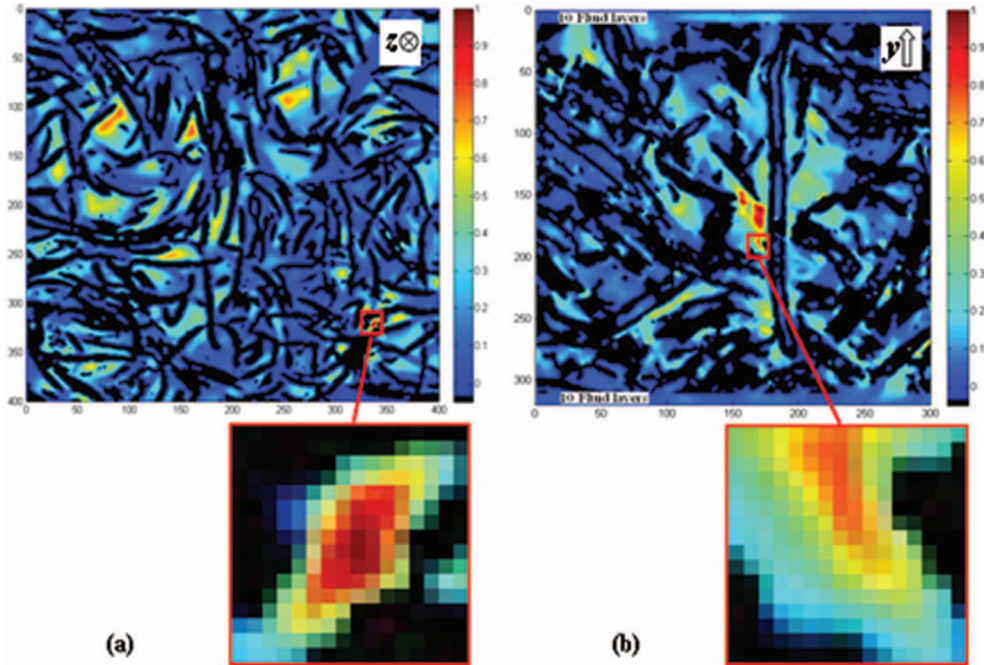


Figure 5. Numerically solved flow field in plastic felt (a) and hardwood paper (b). Shown is the scaled flow speed on single 2D cross sections ( $x$ - $y$  plane) of the full 3D solution space within the actual pore geometry of material subsamples as obtained by X-ray micro-tomography (see Figure 4). Red and blue colours indicate high and low flow velocity, respectively. Solid material is coloured black. In (a) mean velocity is in the direction perpendicular to the plane shown ( $z$  direction). In (b) mean flow is in the plane shown and from up to down ( $y$  direction). Notice also the pure fluid layers visible at the upstream and downstream sides of the paper sample. Inserts show details of the pore structure and flow velocity pattern with resolution of the numerical grid given by the tomographic images ( $4.84 \mu\text{m}$  and  $0.7 \mu\text{m}$  for (a) and (b), respectively). Available in colour online.

Table 1. Numerical and experimental values of permeability in three orthogonal directions (in physical units) for plastic fibre sample and hard wood paper sample.

Sample	Permeability $k_{ij}$ [ $\text{m}^2 \text{E-13}$ ]								
	$k_{xx}$			$k_{yy}$			$k_{zz}$		
	LBM	FDM	Experimental	LBM	FDM	Experimental	LBM	FDM	Experimental
Plastic fibre mat	$290 \pm 10$	352	$311 \pm 9$	$290 \pm 30$	332	$304 \pm 9$	$270 \pm 30$	305	$270 \pm 5$
Hardwood sample	$2.6 \pm 0.3$	2.60	$3.1 \pm 0.1$	$2.7 \pm 0.3$	2.84	$3.1 \pm 0.1$	$0.76 \pm 0.05$	0.85	$0.63 \pm 0.01$

The numerical results obtained with LBM are given as mean values of results based on five non-overlapping subvolumes, and the experimental results as mean values of five independent measurements with standard deviation.

indication of both methods being less accurate in the present complex geometry. Notice that the boundary of the flow domain (pore space) is in this case *known* only to the accuracy of the tomographic image. Therefore, using a numerical grid essentially finer than the voxel matrix of the 3D tomographic digital image does not, in general, improve the overall validity of the solution and of the computed value of permeability coefficient. It is thus obvious that the relatively coarse cubic grid provided directly by the tomographic images does not allow for very accurate solution of flow especially near the solid boundaries and in narrow passages. Nevertheless, the largest

deviation between numerical and experimental results is less than 30%. This is of the same order of magnitude than the overall uncertainty inherent also in the used experimental method for thin compressed fibre mats (Koivu *et al.* 2009a).

The most important single source of uncertainty in the present numerical results most likely is the rather poor statistics obtained due to the low number and small size of (sub)samples. Notice, however, that even though several subsamples were analysed, the variation of permeability value thus obtained (and indicated in Table 1) does not necessarily correspond to the total large scale variation of the sample materials but merely

the variation within the yet rather small original samples scanned. The samples used in experiments are, however, much larger and the results are therefore expected to better represent mean values (apart from possible systematic errors remaining).

### Discussion

In this work we develop and critically evaluate a method for finding flow permeability of porous materials by numerically solving creeping fluid flow through the complex pore space of actual material samples. Two conceptually different numerical schemes, namely LBM and finite difference method were used. The regular cubic grid used in numerical solution is based directly on the 3D images of material samples obtained by two different states of the art X-ray microtomographic techniques.

In many practical cases, the main source of uncertainty within the present approach is the finite resolution of the tomographic image that provides the numerical grid. This may be due to hardware limitations or due to the need of compromising resolution for sample size for heterogeneous materials. The order of magnitude of the discretisation error arising from the relatively sparse numerical grid used was first evaluated solving flows through a set of digitally generated regular geometries of straight cylinders. The values of permeability coefficients were computed using grids of density comparable to that used with actual materials (relative to cylinder/fibre diameter). The results were compared with analytical results available and with more accurate numerical results obtained using grids of sufficiently high density. For the regular geometries studied, the maximum deviation of the results obtained with sparse grid from analytical and more accurate numerical results was less than 10%. This perhaps even surprisingly good accuracy obtained for regular geometries indicates that, as far as discretisation error alone is concerned, the method may be useful also for actual materials. We may, however, expect the discretisation error to be somewhat higher for actual material samples due to their more complex pore structure. Notice also that additional error may arise due to the finite resolution of the tomographic techniques, whereby details of the structure (e.g. surface roughness of fibres and very narrow passages in the porous space) may not be reproduced by the images. Furthermore, noise and other artefacts present in the original reconstructed images as well as image conditioning methods used to remove or minimise them may affect the results for each individual sample. These are the main factors that currently limit the applicability of the method especially for fine-structured materials.

In order to assess the overall uncertainty inherent in the computed results, we applied the method in finding the diagonal components of permeability tensor for two fibrous materials, plastic felt and hand-sheet paper under steady mechanical compression, and compared the results with corresponding experimental values for the same materials. The maximum deviation between the numerical results and the experimental results was found to be less than 30%. In addition to numerical uncertainties arising from discretisation and image quality discussed above, this deviation includes statistical variation arising from relatively small size and low number of samples used in computation. In principle, the accuracy can be improved by using higher resolution tomographic images and better statistics. The former condition may become feasible with the present rapid development of X-ray tomographic techniques. The latter can be obtained by larger size or larger number of samples. Obviously, these improvements come with the cost of higher computational effort which, however, does not appear critical from the point of view of applicability of the method.

To conclude, the method of finding values of flow permeability of porous materials, based on numerically solving fluid flow through the actual 3D pore geometry of material samples found using X-ray micro-tomography, appears useful especially in cases where experimental results are not available or are difficult to obtain. An example of such an application is to find the permeability of various layers in a layer-structured material for which the layers can not be separated for independent measurement (Koivu *et al.* 2009b). Another advantage of the method is that it can be used to find all components of the permeability tensor. With the X-ray tomographic techniques presently used, the overall accuracy of the computed values of permeability is moderate for the kind of materials and flow conditions studied here. However, this uncertainty is not essentially larger than the typical total uncertainty of corresponding experimental results.

Here, we have demonstrated the method in evaluating a particular macroscopic transport property of porous materials, the flow permeability. Similar procedure can be applied in other modes of transport such as diffusion and heat conduction in heterogeneous materials.

### Acknowledgements

The authors thank Tuomas Turpeinen, M.Sc. for his help related to the segmentation of tomographic images, and Jarno Alaraudanjoki, M.Sc. for the work done for experimental permeability measurements. The authors also express their gratitude to the

ID19's team of ESRF for help with the acquisition of the images, and to Sabine Rolland du Roscoat for her enthusiastic help concerning both the acquisition and the image analysis of the studied samples.

## References

- Aaltosalmi, U., *et al.*, 2004. Numerical analysis of fluid flow through fibrous porous materials. *Journal of Pulp and Paper Science*, 30 (9), 251–255.
- Andersson, A.G., *et al.*, 2009. Flow through a two-scale porosity material. *Research Letters in Materials Science*, 2009 (701512), 4 pp.
- Arns, C., *et al.*, 2004. Virtual permeametry on microtomographic images. *Journal of Petroleum Science and Engineering*, 45, 41–46.
- Bear, J., 1972. *Dynamics of fluid in porous media*. New York: Dover Publications inc.
- Belov, E.B., *et al.*, 2003. Modelling of permeability of textile reinforcements: lattice Boltzmann method. *Composites Science and Technology*, 64, 1069–1080.
- Darcy, H., 1856. *Les Fontaines Publiques de la Ville de Dijon*. Paris: Victor Dalmont.
- Drummond, J.E. and Tahir, M.I., 1984. Laminar viscous flow through regular arrays of parallel solid cylinders. *International Journal of Multiphase Flow*, 10 (5), 515–525.
- Eker, E. and Akin, S., 2006. Lattice-Boltzmann simulation of fluid flow in synthetic fractures. *Transport in porous media*, 65, 363–384.
- Fourie, W., *et al.*, 2007. The simulation of pore scale fluid flow with real world geometries obtained from X-ray computed tomography. *European COMSOL Multiphysics Conference*, 23–24 October 2007, Boston. Grenoble: COMSOL inc.
- Frishfelds, *et al.*, 2009. Flow-induced deformation of non-crimp fabrics during composites manufacturing. *Proceedings in Interdisciplinary Transport Phenomena IV (ITP2009)*, Volterra, ITP-09-52.
- Ginzburg, I., 2008. Consistent lattice Boltzmann schemes for the Brinkman model of porous flow and finite Chapman-Enskog expansion. *Physical Review E*, 77, 066704.
- Ginzburg, I. and d'Humières, D., 2003. Multireflection boundary conditions for lattice Boltzmann models. *Physical Review E*, 68 (6), 066614.
- Ginzburg, I., Verhaeghe, F., and d'Humières, D., 2008. Two-relaxation-time lattice-boltzmann scheme: about parametrization, velocity, pressure and mixed boundary conditions. *Communications in Computational Physics*, 3 (2), 427–478.
- Gonzales, R.C. and Woods, R.E., 2001. *Digital image processing*. 2nd edn. New Jersey: Prentice-Hall, Inc, 237–241.
- Hellström, J.G.I. and Lundström, T.S., 2006. Flow through Porous Media at Moderate Reynolds Number, *International Scientific Colloquium: Modelling for Material Processing*, Riga, Latvia, Faculty of Physics and Mathematics, University of Latvia, 129–134.
- Hyvälouma, J., *et al.*, 2006. Simulation of liquid penetration in paper. *Physical Review E*, 73 (3), 036705.
- Jackson, G.W. and James, D.F., 1986. The permeability of fibrous porous media. *Canadian Journal of Chemical Engineering*, 64, 364–373.
- Jaganathan, S., Vahedi Tafreshi, H., and Pourdeyhimi, B., 2007. A realistic approach for modeling permeability of fibrous media: 3-D imaging coupled with CFD simulation. *Chemical Engineering science*, 63 (1), 224–252.
- Keehm, Y., Sternlof, K., and Mukerji, T., 2006. Computational estimation of compaction band permeability in sandstone. *Geosciences Journal*, 10 (4), 499–505.
- Kerwald, D., 2004. Parallel lattice Boltzmann simulation of complex flow. *NAFEMS Seminar: simulation of complex flows (CFD) – applications and trends*. Niedernhausen/Wiesbaden.
- Koivu, V., Mattila, K., and Kataja, M., 2009a. A method for measuring darcian flow permeability of thin fibre mats. *Nordic Pulp and Paper Research Journal*, 24 (4), 395–402.
- Koivu, V., *et al.*, 2009b. Flow permeability of fibrous porous materials. Micro-tomography and numerical simulations. In: S.J. P'Anson, ed. *Advances in pulp and paper research. Transactions on 14th Research Fundamental Symposium*, Oxford, September 14–18, 2009. Manchester: The Pulp and Paper Fundamental Research Society, 437–454.
- Koponen, A., *et al.*, 1998. Permeability of three-dimensional random fiber webs. *Physical Review Letters*, 80 (4), 716.
- Kutay, M.E., Aydilek, A.H., and Masad, E., 2006. Laboratory validation of lattice Boltzmann method for modeling pore-scale flow in granular materials. *Computational Geotechnics*, 33, 381–395.
- Levitz, P., 2005. Toolbox for 3D imaging and modeling of porous media: relationship with transport properties. *Cement and Concrete Research*, 37, 351–359.
- Lundström, T.S., Frishfelds, V., and Jakovics, A., 2004. A statistical approach to permeability of clustered fibre reinforcements. *Journal of Composite Materials*, 38 (13), 1137–1149.
- Lundström, T.S., Sundlöf, H., and Holmberg, J.A., 2006. Modeling of power-law fluid flow through fiber beds. *Journal of Composite Materials*, 40 (3), 283–296.
- Manwart, C., *et al.*, 2002. Lattice-Boltzmann and finite-difference simulations for the permeability for three-dimensional porous media. *Physical Review E*, 66 (1), 016702.
- Martys, N.S. and Hagedorn, J.G., 2002. Multiscale modeling of fluid transport in heterogeneous materials using discrete Boltzmann methods. *Journal of Materials and Structures*, 35 (10), 650.
- Nordlund, M., *et al.*, 2005. Permeability network model for non-crimp fabrics. *Composites Part A*, 37, 826–835.
- Nordlund, M. and Lundström, T.S., 2007. Effect of multi-scale porosity in local permeability modelling of non-crimp fabrics. *Transport in Porous Media*, 73, 109–124.
- Pan, C., Luo, L.-S., and Miller, C.T., 2006. An evaluation of lattice Boltzmann schemes for porous medium flow simulation. *Computers & Fluids*, 35 (8–9), 898.
- Ramaswamy, S., *et al.*, 2004. The 3D structure of fabric and its relationship to liquid and vapor transport. *Colloids and Surfaces A: Physicochemical and Engineering Aspects*, 241, 323–333.
- Rolland du Roscoat, S., Bloch, J.-F., and Thibault, X., 2005. Synchrotron Radiation microtomography applied to paper investigation. *Journal of Physics D: Applied Physics*, 38, A78–A84.
- Rolland du Roscoat, S., *et al.*, 2007. Estimation of microstructural properties from synchrotron X-ray micro tomography and determination of the REV in paper materials. *Acta Materialia*, 55 (8), 2841–2850.

- Saar, M.O. and Manga, M., 1999. Permeability-porosity relationship in vesicular basalts. *Geophysical Research Letters*, 26 (1), 111–114.
- Sangani, A.S. and Acrivos, A., 1982. Slow flow past periodic arrays of cylinders with application to heat transfer. *International Journal of Multiphase Flow*, 8, 193–206.
- Succi, S., 2001. *The lattice Boltzmann equation: for fluid dynamics and beyond*. Gloucestershire: Clarendon Press.
- Succi, S., Foti, E., and Higuera, F., 1989. Three-dimensional flows in complex geometries with the lattice Boltzmann method. *Europhysics Letters*, 10 (5), 432–438.
- Thibault, X. and Bloch, J.-F., 2002. Structural analysis of X-ray microtomography of a strained nonwoven papermaker felt. *Textile Research Journal*, 72 (6), 480–485.
- Verleye, B., *et al.*, 2005. Computation of permeability of textile reinforcements. *Proceedings in Scientific Computation IMACS 2005*, Paris, France.
- Verleye, B., *et al.*, 2007. Permeability of textile reinforcements: simulation, influence of shear and validation. *Composite Science and Technology*, 68 (1), 2804–2810.
- Vidal, D., *et al.*, 2008. Effect of particle size distribution and packing compression on fluid permeability as predicted by lattice-Boltzmann simulations. *Computers and Chemical Engineering*, 33 (1), 256–266.
- White, J.A., Borja, I.R., and Fredrich, J.T., 2006. Calculating the effective permeability of sandstone with multi-scale lattice-Boltzmann/finite element simulations. *Acta Geotechnica*, 1, 195–209.
- Wiegman, A., *et al.*, 2007. Computation of the permeability of porous materials from their microstructure by FFT-stokes. Report of the Fraunhofer ITWM, 129.